

Singular perturbation theory and convergence of equation-free analysis methods

Jan Sieber

These notes are based on the convergence results in [Marschler et al., 2013] (included in the folder papers).

Contents

1 Motivating example — SIS network with reconnection	1
2 Fenichel's Theorem	3
3 Equation-free analysis	6
4 Feasibility conditions for equation-free analysis	8
5 The flow on \mathcal{C}_ε in restricted coordinates	9
6 Approximating the flow on \mathcal{C}_ε with equation-free analysis	11
7 Modification of the practical formulas for equation-free analysis	13
8 Discussion of the convergence statements	14
9 Test examples	15
9.1 A prototype slow-fast system of ODEs	15
9.2 Investigation of dependence on L and R	17

1 Motivating example — SIS network with reconnection

Let us consider an example close to the true motivation of equation-free analysis for a multi-scale system. Gross et al. [2006] consider the spread of a disease on a network of

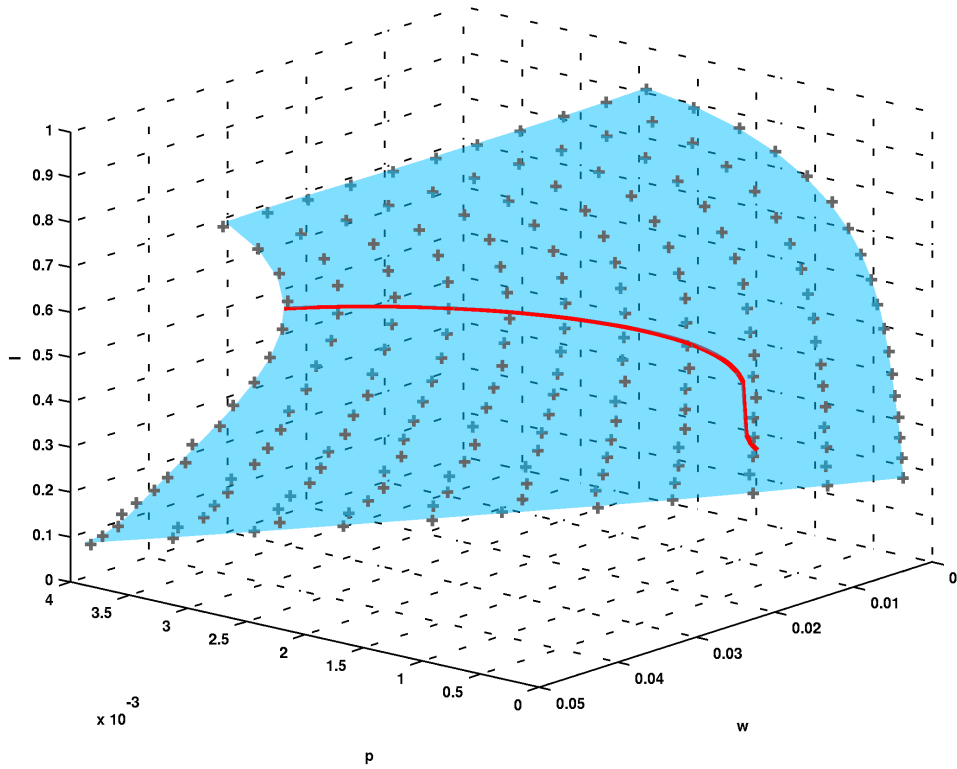


Figure 1: Family of endemic equilibria and their fold for the SIS network with rewiring ($N = 4000$ individuals) in the (p, w, I) -space. Grey crosses: equilibria as computed by simulation of network; blue surface: surface of equilibria as interpolated with regression from the equilibria. Red curve: saddle-node bifurcation, determined as the fold of the blue equilibrium surface.

N individuals, corresponding to nodes in a network ($N = 10^4$ in Gross et al. [2006]), which are initially randomly connected (with average node degree $k = 10$). There exists two types of individuals, infected I and susceptible S . Initially a random sample of i individuals is infected (fraction $I = i/N$), the others are assigned the status of susceptible fraction $S = (1 - i/N)$. At every time step every infected node recovers (turning into a susceptible) with probability r ($r = 0.002$ in Gross et al. [2006]). For every SI link (between an infected and a susceptible node) the disease gets transmitted along the link with probability p (a bifurcation parameter varying between 0 and 0.008 in Gross et al. [2006]). In addition, at every step every SI link is broken up with probability w (w varies between 0 and 0.2 in Gross et al. [2006]). This break-up occurs such that the S node of the link removes the link to the I node and instead connects to a random other susceptible node (avoiding self links and double links, and preserving the overall number of links).

One observation is that for w greater some w_c and a certain range of p a stable

disease free state and a stable equilibrium with an endemic disease (that is a large fraction I of infected individuals) coexist. Gross et al. [2006] derive a three-dimensional ODE that serves as an approximation for the behavior of the network. The variables are I (the fraction of infected individuals), ℓ_{II} , the density of links between infected individuals, and ℓ_{SS} , the density of links between susceptible individuals. The equations are

$$\frac{d}{dt}I = p\ell_{SI} - rI, \quad \frac{d}{dt}\ell_{II} = p\ell_{SI} \left[\frac{\ell_{SI}}{S} + 1 \right] - 2r\ell_{II}, \quad \frac{d}{dt}\ell_{SS} = (r + w)\ell_{SI} - \frac{2p\ell_{SI}\ell_{SS}}{S}, \quad (1)$$

where we know that $S = 1 - I$ and $\ell_{SI} = k/2 - \ell_{SS} - \ell_{II}$. The approximation is valid when the network has a certain degree of uniformity, that is, triangles of type a - b - c occur with frequency $\ell_{ab}\ell_{bc}/b$ (where $a, b, c \in \{S, I\}$). This type of approximation is called a *closure approximation*. One replaces unknown terms by functions of already included dependent variables.

Gross et al. [2006] find that, for the ODE (1), the coexistence region is bounded by a classical fold (saddle-node) of the endemic equilibrium and a transcritical bifurcation of the disease-free state. The two are separated by an unstable equilibrium with non-zero fraction of infected, I . The question is, can one, without making the closure approximation, by direct simulations of the network from appropriately chosen initial conditions. Figure 1 shows that this is in principle possible. Gross and Kevrekidis [2008] demonstrate Kevrekidis' equation-free approach as discussed in this lecture for a network with similar rules.

2 Fenichel's Theorem

Fenichel's Theorem should have shown up in earlier sessions (possibly with different notation). The re-statement here is a simplified version for the special case of *transversally stable* slow manifolds.

Let

$$\dot{u} = F_\varepsilon(u) \quad (2)$$

be a smooth dynamical system defined for $u \in \mathbb{R}^N$, which depends smoothly on the parameter ε . All conditions on the system will be stated for $\varepsilon = 0$.

Condition S1: compact manifold of equilibria at $\varepsilon = 0$ We assume that ε is a *singular perturbation parameter*. This means that the flow M_ε generated by (2),

$$M_\varepsilon : (t; u) \in \mathbb{R} \times \mathbb{R}^N \mapsto M_\varepsilon(t; u) \in \mathbb{R}^N,$$

has a whole smooth n -dimensional submanifold \mathcal{C}_0 of equilibria for $\varepsilon = 0$: if $u \in \mathcal{C}_0$ then $M_0(t; u) = u$ for all t (and, thus, $F_0(u) = 0$). This scenario is clearly singular in some sense as one would generically expect equilibria to be isolated. To avoid discussion of what happens on the boundaries of \mathcal{C}_0 , we assume that \mathcal{C}_0 is compact. In the notation of singular perturbation theory, t measures time on the *fast* time scale.

Condition S2: uniform transversal stability Moreover, we assume that this manifold \mathcal{C}_0 is transversely uniformly exponentially stable for $\varepsilon = 0$, corresponding to the *stable* case of Fenichel's geometric singular perturbation theory [Fenichel, 1979]. Let us denote the Jacobian of F_ε in u as $\partial F_\varepsilon(u)$. Then the value 0 is an eigenvalue of $\partial F_0(u)$ with geometric multiplicity n for u in the manifold of equilibria \mathcal{C}_0 . The nullspace $\mathcal{T}_0(u)$ of $\partial F_0(u)$ is the tangent space to \mathcal{C}_0 in u (see Fig. 2a). We require that all $N - n$ other eigenvalues of $\partial F_0(u)$ are in the left half plane uniformly for all $u \in \mathcal{C}_0$. That is, we assume that there exists a spectral gap $\gamma_0 > 0$ such that

$$\operatorname{Re} \lambda < -\gamma_0 \quad \text{for all } \lambda \in \operatorname{spec} \partial F_0(u) \setminus \{0\} \text{ and all } u \in \mathcal{C}_0. \quad (3)$$

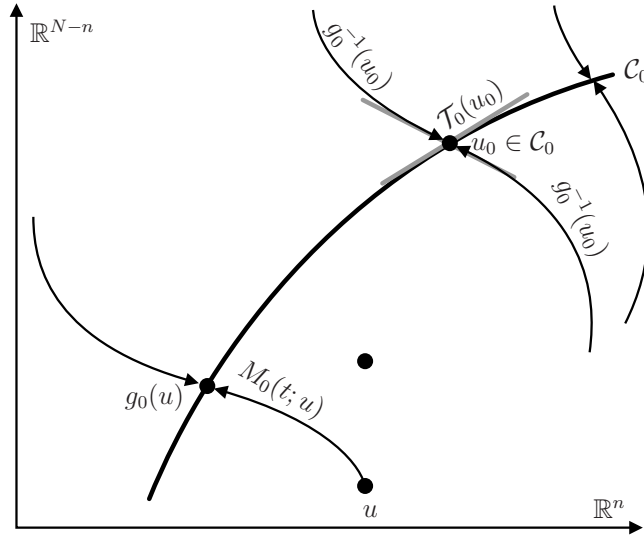


Figure 2: Sketch of the assumptions on the geometry for $\varepsilon = 0$.

Consequence 0: stable foliation A consequence of the above two assumptions is that for $\varepsilon = 0$ there exists an open neighborhood \mathcal{U} of \mathcal{C}_0 , which is *foliated by stable fibers*. More precisely, the flow M_0 converges to the slow manifold \mathcal{C}_0 with a uniform rate γ_0 (the spectral gap) from all initial conditions $u \in \mathcal{U}(\mathcal{C}_0)$. That is, for every $u \in \mathcal{U}$ there exists a point $p \in \mathcal{C}_0$ such that

$$\lim_{t \rightarrow \infty} M_0(t; u) = p$$

(note that for $\varepsilon = 0$ all points on the manifold \mathcal{C}_0 are equilibria of M_0), and the distance can be bounded via

$$\|M_0(t; u) - p\| \leq C \exp(-\gamma_0 t) \|u - p\|, \quad \|\partial_2^j M_0(t; u)\| \leq C \exp(-\gamma_0 t)$$

for all $t \geq 0$ and $j \geq 1$, where the constant C depends only on the derivative order j , but is uniform for all $u \in \mathcal{U}(\mathcal{C}_0)$. The above statement implies the existence of a smooth map (called the *stable fiber projection*)

$$g_0 : \mathcal{U} \rightarrow \mathcal{C}_0, \quad \text{defined by} \quad g_0(u) := p, \quad (4)$$

assigning to each u its limit $p \in \mathcal{C}_0$ under the flow M_0 (see Figure 2).

Consequence 1: persistence of slow manifold The slow manifold \mathcal{C}_0 persists for sufficiently small ε , deforming to a smooth nearby manifold \mathcal{C}_ε (as shown in Figure 3). Restricted to \mathcal{C}_ε the flow is governed by a smooth ODE (the *slow* flow) with a right-hand side for which all derivatives up to a given order k are proportional to ε (larger k requires smaller ε):

$$\|f_\varepsilon(u)\| \leq C\varepsilon, \quad \|\partial^j f_\varepsilon(u)[v_1, \dots, v_j]\| \leq C\varepsilon \|v_1\| \cdots \|v_j\| \quad (5)$$

for all $j = \{1, \dots, k\}$, $u \in \mathcal{C}_\varepsilon$ and v_1, \dots, v_j in the tangent space $\mathcal{T}_\varepsilon(u)$ of \mathcal{C}_ε (for $\varepsilon = 0$ the space $\mathcal{T}_0(u)$ is the null space of the linearization $\partial F_0(u)$). The constants C are independent of u . Thus, the flow $M_\varepsilon(t; \cdot)$ is a global diffeomorphism on the slow manifold \mathcal{C}_ε which has growth bounds of order ε forward and backward in time:

$$\|\partial_2^j M_\varepsilon(t; \cdot)|_{\mathcal{C}_\varepsilon}\| \leq C \exp(\varepsilon|t|), \quad \|\partial_2^j M_\varepsilon^{-1}(t; \cdot)|_{\mathcal{C}_\varepsilon}\| \leq C \exp(\varepsilon|t|), \quad (6)$$

for some constant C independent of t and ε and all derivative orders j up to a fixed order k . Note that $M_\varepsilon^{-1}(t; \cdot) = M_\varepsilon(-t; \cdot)$ for all times t as long as one restricts the flow M_ε to the slow manifold \mathcal{C}_ε .

Consequence 2: persistence of stable fibers We assume that ε is sufficiently small such that the perturbed manifold \mathcal{C}_ε is still a subset of the neighborhood \mathcal{U} of the original unperturbed manifold \mathcal{C}_0 . Then the stable fiber projection map g_0 persists for small ε , getting perturbed smoothly to a map g_ε , defined for each u in the neighborhood \mathcal{U} of the manifold \mathcal{C}_0 (and its perturbation \mathcal{C}_ε). The map g_ε picks for every point $u \in \mathcal{U}$ the unique point $g_\varepsilon(u)$ inside the slow manifold \mathcal{C}_ε such that the trajectories starting from u and $g_\varepsilon(u)$ converge to each other forward in time with an exponential rate γ of order 1 (that is, γ is uniformly positive for all sufficiently small ε and all $u \in \mathcal{U}$):

$$\begin{aligned} \|M_\varepsilon(t; u) - M_\varepsilon(t; g_\varepsilon(u))\| &\leq C \exp(-\gamma t) \|u - g_\varepsilon(u)\|, \\ \|\partial_2^j M_\varepsilon(t; u) - \partial_2^j M_\varepsilon(t; g_\varepsilon(u))\| &\leq C \exp(-\gamma t) \|u - g_\varepsilon(u)\|, \end{aligned} \quad (7)$$

for all $t \geq 0$, $u \in \mathcal{U}$ and $0 \leq j \leq k$, where the constant C is uniform for $u \in \mathcal{U}$. In general, the decay rate γ has to be slightly smaller than spectral gap γ_0 asserted to exist in Condition S1 for $\varepsilon = 0$. More precisely, for every rate $\gamma < \gamma_0$ there exists a range $(0, \varepsilon_0)$ of ε for which (7) holds. Choosing ε_0 smaller permits one to choose γ closer to γ_0 .

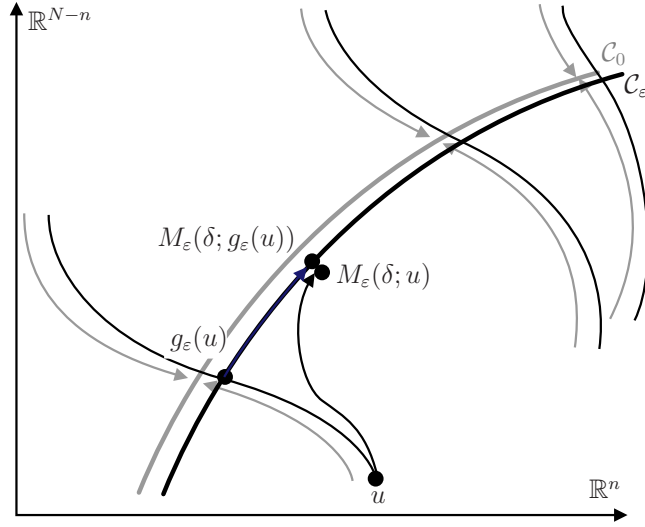


Figure 3: Geometry for $\varepsilon > 0$. The singular case $\varepsilon = 0$ from Fig. 2 is gray in the background. A trajectory of length (time) δ starting from u and its shadow trajectory on \mathcal{C}_ε are shown.

In (7) the notation $\partial_2^j M_\varepsilon$ refers to the j th-order partial derivative of the flow M_ε with respect to its second argument (the starting point). The stable fiber projection map g_ε is an order- ε perturbation of g_0 :

$$\|g_\varepsilon(\mathbf{u}) - g_0(\mathbf{u})\| \leq C\varepsilon, \quad \|\partial^j g_\varepsilon(\mathbf{u}) - \partial^j g_0(\mathbf{u})\| \leq C\varepsilon \quad (8)$$

for all $j = \{1, \dots, k\}$ and a constant C that is uniform for all $\mathbf{u} \in \mathcal{U}$. The black curves transversal to \mathcal{C}_ε in Figure 3 illustrate the fibers, that is, which points of \mathcal{U} get mapped onto the same point in \mathcal{C}_ε under g_ε . Note that the fibers are not trajectories of the flow M_ε for $\varepsilon > 0$.

Note that the stable foliation permits us to extend the definition of $\mathcal{T}_\varepsilon(\mathbf{u})$ trivially to points $\mathbf{u} \in \mathcal{U}$ that are not elements of the slow manifold \mathcal{C}_ε :

$$\mathcal{T}_\varepsilon(\mathbf{u}) := \mathcal{T}_\varepsilon(g_\varepsilon(\mathbf{u})). \quad (9)$$

3 Equation-free analysis

The equation-free approach to coarse graining, originally proposed by Kevrekdis (see Kevrekdis and Samaey [2010] for a Scholarpedia entry and Kevrekdis and Samaey [2009] for a recent review) does not require direct access to the right-hand side F of (2) but merely the ability to evaluate $M_\varepsilon(t; \mathbf{u})$ for finite positive times t and arbitrary \mathbf{u} . Typically, $1 \ll t \ll 1/\varepsilon$ in the fast time scale t , used in our notation. It also relies on two

smooth (possibly linear) maps that have to be chosen beforehand

$$\begin{aligned} R : \mathbb{R}^N &\mapsto \mathbb{R}^n && \text{the restriction map,} \\ L : \mathbb{R}^n &\mapsto \mathbb{R}^N && \text{the lifting map.} \end{aligned}$$

The basic idea underlying equation-free analysis is that one can explore many aspects of the dynamics of (2) on the slow manifold \mathcal{C}_ε by studying a map in the space of restricted variables $x \in \text{dom } L$ (the domain of L) of the form

$$\text{Lift} \mapsto \text{Time-step} \mapsto \text{Restrict},$$

or, to be precise, the map

$$P_\varepsilon(t, \cdot) : \mathbb{R}^n \mapsto \mathbb{R}^n, \quad \text{given by } x \mapsto \text{RM}_\varepsilon(t; Lx). \quad (10)$$

In the notation of [Kevrekidis and Samaey \[2009\]](#), the evaluation of $M_\varepsilon(t; u)$ for an initial value $u \in \mathbb{R}^n$ is called a *microscopic simulator*.

The idea behind this notion is that one can treat many-particle systems with a large number of degrees of freedom (*microscopic systems*) as slow-fast systems, where the random microscopic motion averages out and macroscopic quantities move on the slow time scale. The relaxation occurs only in a statistical mechanics sense toward an equilibrium. Section 1 will give a practical example.

Finding equilibria For example, [Kevrekidis and Samaey \[2009\]](#) propose that one can find equilibria of (2) approximately by solving

$$P_\varepsilon(t; x) = x \quad (11)$$

for x where $t > 0$ is an appropriately chosen time. Generally, $1 \ll t \ll 1/\varepsilon$ is chosen. This guarantees that, after lifting x to Lx , the flow $M_\varepsilon(t; Lx)$ has converged to the slow manifold \mathcal{C}_ε (implied by (7)). Thus, the time t has to be long enough to contain the *initial layer* of the trajectory $M_\varepsilon([0, t]; Lx)$ (the exponentially decaying part off the slow manifold).

The other restriction on t , $t \ll 1/\varepsilon$, is imposed by the time scale on the slow manifold. The derivatives of the flow M_ε restricted to the slow manifold are of order ε such that integration times of order less than $1/\varepsilon$ can be considered short ([Kevrekidis and Samaey \[2009\]](#) call the integration for time t a short burst of simulation).

Stability Correspondingly, the stability and bifurcations of an equilibrium x_0 can be found by studying the Jacobian of P_ε ,

$$J_\varepsilon(t; x_0) = \frac{\partial}{\partial x} P_\varepsilon(t; x)|_{x=x_0} = \frac{\partial}{\partial x} [\text{RM}_\varepsilon(t; Lx)]|_{x=x_0}.$$

Projective integration One can also perform numerical integration on the slow manifold with time steps different from the time steps in the simulator. Suppose one has an initial value $x(0) = x_0$ for the restricted variables in $\text{dom } L$. For example, one first calculates

$$f_{\text{approx}}(x_0) = \frac{1}{h} [P_\varepsilon(h; x_0) - x_0]$$

as an approximation of the derivative of the right-hand side of the flow on the slow manifold \mathcal{C}_ε , and then one performs an explicit Euler step with step size $H \neq h$ to obtain

$$x(h) = x_0 + H f_{\text{approx}}(x_0).$$

Projective integration is of interest if one can either choose $H \gg h$. Remember that x is supposed to follow the dynamics on the slow manifold, where the true right-hand side f_ε is small (see (5)). Another scenario of potential interest is integration backward in time (choosing $H < 0$). Backward integration is practically impossible in the full system because it is stiff, and, thus, strongly expanding backward in time. However, on the slow manifold \mathcal{C}_ε the flow is invertible with more moderate growth (again, (5)).

4 Feasibility conditions for equation-free analysis

The restriction R and the lifting L have to satisfy a few conditions to make equation-free analysis feasible (not yet attempting to prove convergence in any sense). Again, the conditions will be formulated for $\varepsilon = 0$. They will then automatically hold for sufficiently small $\varepsilon > 0$.

Condition M1: transversality for the lifting L First of all L has to map into the neighborhood \mathcal{U} of \mathcal{C}_0 :

$$L : \text{dom } L \subset \mathbb{R}^n \mapsto \mathcal{U}. \quad (12)$$

However, this is not enough. The idea behind equation-free analysis is that our restricted variables $x \in \text{dom } L$ can be used as coordinates on the slow manifold \mathcal{C}_ε . Hence, we have to require some kind of transversality. One sensible transversality condition is to assume that the stable fiber projection g_0 provides a (local) diffeomorphism between $\text{rg } L$ and \mathcal{C}_0 . Equivalently, the Jacobian matrix of $g_0 \circ L$ has to have full rank:

$$\text{rank}[\partial g_0(Lx) \circ \partial L(x)] = n \quad \text{for all } x \in \text{dom } L. \quad (13)$$

This assumption is reasonable. It assumes that, in the limit of infinite time-scale separation ($\varepsilon = 0$), nearby but different points x_1 and x_2 in the space of restricted variables $\text{dom } L$ get mapped onto different (but nearby) points $g_0(Lx_1)$ and $g_0(Lx_2)$ in \mathcal{C}_0 . Figure 4(b) shows how a violation of this rule would look like for $n = 1$ and $N = 3$.

A direct consequence is that this transversality condition is also satisfied for small $\varepsilon > 0$:

$$\text{rank}[\partial g_\varepsilon(Lx) \circ \partial L(x)] = n \quad \text{for all } x \in \text{dom } L. \quad (14)$$

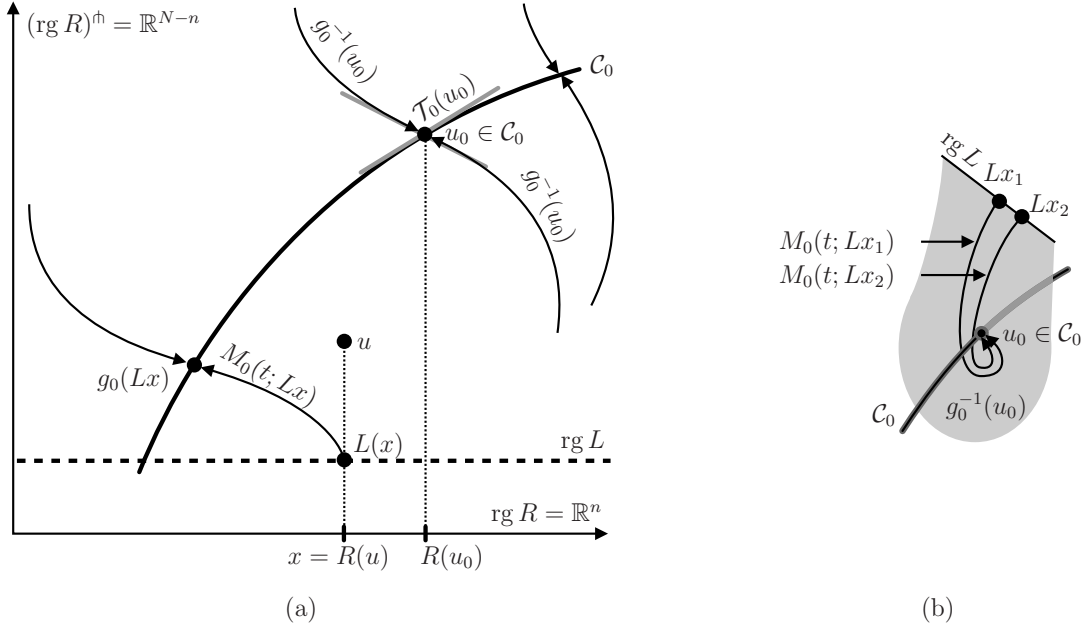


Figure 4: Sketch illustrating the transversality assumptions on R and M for $\varepsilon = 0$. (a) General setup, (b): Condition M1, no two points from the range of L should be projected onto the point of \mathcal{C}_0 by the fiber.

Condition M2: Transversality for the restriction R The restriction R has to be defined on the neighborhood \mathcal{U} of \mathcal{C}_0 (which also contains all slow manifolds \mathcal{C}_ε for all ε under consideration): $R : \mathcal{U} \mapsto \mathbb{R}^n$.

In addition we have to require that the restriction R does not collapse nearby points on \mathcal{C}_0 onto the same image. More precisely, R has to be a local diffeomorphism from \mathcal{C}_0 to $\text{rg } R \subset \mathbb{R}^n$. Equivalently, this means that the dimension of the space $\partial R(u)\mathcal{T}_0(u)$ equals n for all $u \in \mathcal{C}_0$. Remember that $\mathcal{T}_0(u)$ is the tangent space of \mathcal{C}_0 in $u \in \mathcal{C}_0$ (and the nullspace of $\partial F_0(u)$).

Again, a direct consequence is that this transversality condition is also satisfied for small $\varepsilon > 0$:

$$\dim[\partial R(u)\mathcal{T}_\varepsilon(g_\varepsilon(u))] = n \quad \text{for all } u \in \mathcal{U} \text{ sufficiently close to } \mathcal{C}_\varepsilon. \quad (15)$$

5 The flow on \mathcal{C}_ε in restricted coordinates

The conditions M1 and M2 permit us to express the flow M_ε , restricted to the slow manifold \mathcal{C}_ε for $\varepsilon > 0$, in the restricted coordinates $x \in \text{dom } L$. In order to be able to write an ODE on the manifold \mathcal{C}_ε we need a chart for \mathcal{C}_ε in $\text{dom } L$.

The following map $X_{0,\varepsilon} : \text{dom } L \mapsto \mathcal{C}_\varepsilon$ is such a chart for (a part of) \mathcal{C}_ε over $\text{dom } L$:

$$X_{0,\varepsilon}(x) = g_\varepsilon(Lx).$$

Why is this map is locally invertible? Because $g_0 \circ L$ is a local diffeomorphism between $\text{dom } L$ and \mathcal{C}_0 by assumption **M1**. Thus, the perturbation $g_\varepsilon \circ L$ is a diffeomorphism between $\text{dom } L$ and \mathcal{C}_ε for small ε as stated in (14).

How can one compute the local inverse of this map in practice? Let us assume, we are given a point $u_{\text{ref}} \in \mathcal{C}_\varepsilon$ and its pre-image $x_{\text{ref}} \in \text{dom } L$ ($g_\varepsilon(Lx_{\text{ref}}) = u_{\text{ref}}$). How can one find the pre-image $x \approx x_{\text{ref}}$ of a point $u \approx u_{\text{ref}}$ in \mathcal{C}_ε ? We can solve the regular nonlinear system

$$Rg_\varepsilon(Lx) = Ru. \quad (16)$$

The combination of the assumptions **M1** and **M2** ensures that the Jacobian of the left-hand side with respect to x is regular, and for $u = u_{\text{ref}}$ we have a solution x_{ref} .

Since the restriction R defines the inverse of the local diffeomorphism between $\text{dom } L$ and \mathcal{C}_ε implicitly, the flow on \mathcal{C}_ε follows an implicit ODE for x :

$$\frac{d}{dt} [Rg_\varepsilon(Lx)] = RF_\varepsilon(g_\varepsilon(Lx)). \quad (17)$$

This ODE is an exact representation of the flow M_ε in x coordinates in $\text{dom } L$. This representation is not practically useful because g_ε and F_ε are not known. The evaluation of F_ε can be approximated by a time step difference of a numerical integration (say, $F_\varepsilon(u) \approx (M_\varepsilon(h; u) - u)/h$ for small h). However, the fiber projection g_ε , which is needed to project Lx onto \mathcal{C}_ε , is beyond reach.

An equivalent representation There are various ways to overcome the inaccessibility of the stable fiber projection g_ε . One way is to ensure that L always maps onto the slow manifold \mathcal{C}_ε . The procedure described by Zagaris et al. [2009, 2012] achieves this approximately to finite order of ε . We take another approach, achieving exponentially accurate $\sim \exp(-C/\varepsilon)$ convergence.

Apparently, for $\delta = T/\varepsilon$ and $T > 0$ fixed, the flow $u \mapsto M_\varepsilon(\delta; u)$ is a global diffeomorphism on \mathcal{C}_ε . In fact, $M_\varepsilon(\delta; \cdot)$ is a perturbation of the identity of order T due to (5). Hence, the concatenation of the map $X_{0,\varepsilon}(x) = g_\varepsilon(Lx) : \text{dom } L \mapsto \mathcal{C}_\varepsilon$ with the diffeomorphism $M_\varepsilon(\delta; \cdot)$ is also local diffeomorphism between $\text{dom } L$ and \mathcal{C}_ε :

$$X_{\delta,\varepsilon}(x) := M_\varepsilon(\delta; g_\varepsilon(Lx)). \quad (18)$$

The local diffeomorphisms $X_{\delta,\varepsilon}$ provide a family of charts for \mathcal{C}_ε over $\text{dom } L$, parametrized with δ . Each of these charts will give a different form for the implicit ODE. However, all these different ODEs will be identical except for a change of coordinates.

The local inverse of $X_{\delta,\varepsilon}$ can be computed implicitly in the same way as the inverse of $X_{0,\varepsilon}$: let us assume, we are given a point $u_{\text{ref}} \in \mathcal{C}_\varepsilon$ and its pre-image $x_{\text{ref}} \in \text{dom } L$ ($M_\varepsilon(\delta; g_\varepsilon(Lx_{\text{ref}})) = u_{\text{ref}}$). How can one find the pre-image $x \approx x_{\text{ref}}$ of a point $u \approx u_{\text{ref}}$ in \mathcal{C}_ε ? We can solve the regular nonlinear system

$$RM_\varepsilon(\delta; g_\varepsilon(Lx)) = Ru. \quad (19)$$

All parts of the left-hand side are known to be local diffeomorphisms: $g_\varepsilon \circ L : \text{dom } L \mapsto \mathcal{C}_\varepsilon$, $M_\varepsilon(\delta; \cdot) : \mathcal{C}_\varepsilon \mapsto \mathcal{C}_\varepsilon$, and $R : \mathcal{C}_\varepsilon \mapsto \mathbb{R}^n$ (using the assumptions **M1** and **M2**). This ensures that the Jacobian of the left-hand side with respect to x is regular. Moreover, for $u = u_{\text{ref}}$ we have a solution x_{ref} such that we can apply the inverse function theorem to solve (19).

In this modified coordinate representation the flow on the slow manifold is governed by implicit ODE for x :

$$\frac{d}{dt} [\text{RM}_\varepsilon(\delta; g_\varepsilon(Lx))] = \text{RF}_\varepsilon(M_\varepsilon(\delta; g_\varepsilon(Lx))). \quad (20)$$

Again, this ODE is an exact representation of the flow M_ε in x coordinates in $\text{dom } L$. Notice that the only difference to the ODE (17) using only the fiber projection is the insertion of the diffeomorphism $M_\varepsilon(\delta; \cdot)$ in front of g_ε (that is, the diffeomorphism $M_\varepsilon(\delta; \cdot)$ is applied after g_ε).

Implicit flow map Φ_* Instead of writing an implicit ODE we can also define the flow map $\Phi_* : [0, \infty) \times \text{dom } L \mapsto \text{dom } L$, which is a representation of the flow M_ε , restricted to \mathcal{C}_ε in the coordinates in $\text{dom } L$. For $t \in [0, T_{\text{up}}/\varepsilon]$ with sufficiently small T_{up} , $\Phi_*(t; x)$ is given implicitly as the solution y_* of

$$\text{RM}_\varepsilon(\delta + t; g_\varepsilon(Ly_*)) = \text{RM}_\varepsilon(\delta + t; g_\varepsilon(Lx)), \quad (21)$$

For larger t we split up t into m smaller time steps and define

$$\Phi_*(t; x) := \Phi_*(t/m; \cdot)^m[x]. \quad (22)$$

(However, in the context of equation-free analysis we are typically interested in short times t .) Obtaining $\Phi_*(t; \cdot)$ for small negative t can be reduced to solving the same nonlinear system (21), swapping x and y_* .

6 Approximating the flow on \mathcal{C}_ε with equation-free analysis

The flow Φ_* is the exact flow map for M_ε , restricted to \mathcal{C}_ε , written in the x coordinates in $\text{dom } L \subset \mathbb{R}^n$, and using the local diffeomorphism $M(\delta; g_\varepsilon(L \cdot)) : \text{dom } L \mapsto \mathcal{C}_\varepsilon$ to define the chart of the manifold \mathcal{C}_ε .

In the defining equation (21) for Φ_* , the only unknown map is g_ε . However, when we replace $M(\delta; g_\varepsilon(\cdot))$ by $M_\varepsilon(\delta; \cdot)$ we make an exponentially small error, and we obtain a defining equation for an approximate flow map $\Phi : [0, \infty) \times \text{dom } L \mapsto \text{dom } L$. The solution y of the system

$$\text{RM}_\varepsilon(\delta; Ly) = \text{RM}_\varepsilon(\delta + t; Lx) \quad (23)$$

is the image of x : $\Phi(t; x) := y$. The extension to larger times t and negative t is identical to the definition for Φ_* .

In which sense is the error exponentially small? The exponential contraction along fibers, stated in (7) ensures that

$$\begin{aligned} \|M_\varepsilon(\delta; Lx) - M_\varepsilon(\delta; g_\varepsilon(Lx))\| &\leq C \exp(-\gamma\delta) \|Lx - g_\varepsilon(Lx)\| \leq \tilde{C} \exp(-\gamma\delta), \\ \|\partial_2^j M_\varepsilon(\delta; Lx) - \partial_2^j M_\varepsilon(\delta; g_\varepsilon(Lx))\| &\leq C \exp(-\gamma\delta) \|Lx - g_\varepsilon(Lx)\| \leq \tilde{C} \exp(-\gamma\delta), \end{aligned} \quad (24)$$

where we estimated $Lx - g_\varepsilon(Lx)$ with a constant (the constant \tilde{C} is independent of x and ε for x in a bounded region). Since δ was of the form T/ε for a fixed T (T is measuring time on the slow time scale), we obtain that the nonlinear maps on both sides of the defining system (21) for Φ_* (the exact flow map) and of the defining system (23) for the approximate flow map Φ differ by a term of the form

$$C \exp(-\gamma T/\varepsilon)$$

in all derivatives up to a finite order k , where C is independent of x and ε . This ensures that the solutions Φ_* and Φ also differ by a term of the same form.

The error estimates (24) highlight the purpose of the time shift δ along the slow flow on the manifold \mathcal{C}_ε . Choosing it larger than 0 “heals” the error committed by lifting x to a point away from the slow manifold \mathcal{C}_ε . The concept of a *healing time* is also mentioned in the review [Kevrekidis and Samaey, 2009], but δ is included only on the right-hand side of (23) there.

We can collect our statements in the following theorem:

Theorem 1 (Convergence of equation-free analysis)

Let $T > 0$ and $T_{\text{up}} > 0$ be fixed and sufficiently small, and let $D \subset \text{dom } L$ be a bounded set. Let the two maps Φ_* and Φ be defined implicitly for $t \in [0, T_{\text{up}}/\varepsilon]$ by

$$\begin{aligned} \text{RM}_\varepsilon(T/\varepsilon; g_\varepsilon(Ly_*)) \text{RM}_\varepsilon(T/\varepsilon + t; g_\varepsilon(Lx)), & \quad \Phi_*(t; x) := y_*, \\ \text{RM}_\varepsilon(T/\varepsilon; Ly) = \text{RM}_\varepsilon(T/\varepsilon + t; Lx), & \quad \Phi(t; x) := y. \end{aligned}$$

Then the difference between the two maps is bounded by

$$\begin{aligned} \|\Phi(t; x) - \Phi_*(t; x)\| &\leq C \exp(-\gamma/\varepsilon), \\ \|\partial_2^j \Phi(t; x) - \partial_2^j \Phi_*(t; x)\| &\leq C \exp(-\gamma/\varepsilon) \quad \text{for all } j \in \{1, \dots, k\}. \end{aligned} \quad (25)$$

The constants C in the estimate depend on T and T_{up} and the domain D , but not on x and ε .

Note that the bound T_{up} for the time t is only sufficiently small on the slow time scale.

7 Modification of the practical formulas for equation-free analysis

The fact that the flow map Φ_* is in fact implicitly defined, requires a few modifications of the formulas presented in Section 3.

Suppose, we are given the maps for restriction R , lifting L and a time-stepper $M_\varepsilon(t; \cdot)$. Then one can perform a number of tasks by solving low-dimensional nonlinear systems. In the following formulas the healing time δ has to be chosen sufficiently large (what this means in a given example has to be determined by experimentation).

Finding equilibria boils down to finding fixed points of $\Phi(t; \cdot)$ with some (fairly arbitrary) t . Typically, one has to choose t small on the slow time scale, that is, $t = T_{\text{step}}/\varepsilon$ where T_{step} is small, but may not necessarily be small. Hence, equilibria can be found by solving the regular n -dimensional system

$$RM_\varepsilon(\delta + t; Lx) = RM_\varepsilon(\delta; Lx) \quad (26)$$

for $x \in \text{dom } L$. This equation has been proposed and studied already in [Vandekerckhove et al., 2011]. Typically, this task is performed with a Newton iteration (or one of its modifications), and a pseudo-arclength continuation.

Stability of equilibria Correspondingly, the stability and bifurcations of an equilibrium x_0 can be found by studying the generalized eigenvalue problem

$$\left[\frac{\partial}{\partial x} [RM_\varepsilon(\delta + t; Lx)] \Big|_{x=x_0} \right] x = \lambda \left[\frac{\partial}{\partial x} [RM_\varepsilon(\delta; Lx)] \Big|_{x=x_0} \right] x. \quad (27)$$

This eigenvalue problem will give the eigenvalues of the implicitly-known flow map $\Phi(t; \cdot)$ linearized in the equilibrium x_0 such that bifurcations occur when λ is on the unit circle.

Projective integration Since the flow on \mathcal{C}_ε is available only in implicit form, every integration scheme becomes implicit. For example, if one wants to perform an explicit Euler step of stepsize H starting from x_j at time t_j , this is equivalent to the implicit scheme (defining x_{j+1} as the new value at time $t_{j+1} = t_j + H$):

$$RM_\varepsilon(\delta; Lx_{j+1}) - RM_\varepsilon(\delta; Lx_j) = \frac{H}{h} [RM_\varepsilon(\delta + h; Lx_j) - RM_\varepsilon(\delta; Lx_j)]. \quad (28)$$

In (28), we have approximated the right-hand side of the ODE of the slow flow by a finite-difference approximation:

$$F_\varepsilon(u) \approx \frac{1}{h} [M_\varepsilon(h; u) - u]$$

for $u = M_\varepsilon(\delta; Lx)$.

Matching the restriction Sometimes it is of interest to find a microscopic state $u \in \mathbb{R}^N$ on the slow manifold \mathcal{C}_ε that has a particular $x \in \mathbb{R}^n$ as its restriction ($Ru = x$), see [Gear et al., 2005, Zagaris et al., 2009, 2012]. This state u is defined implicitly, and can be found by solving the n -dimensional nonlinear equation

$$RM_\varepsilon(\delta; L\tilde{x}) = x \quad (29)$$

for \tilde{x} , and then setting $u = M_\varepsilon(\delta; L\tilde{x})$. This solution u is close to the true slow manifold \mathcal{C}_ε with an error of order $\exp(-\gamma\delta)$. This implies that, if we choose $\delta = T/\varepsilon$ with a fixed small $T > 0$, the distance of u to \mathcal{C}_ε is small beyond all orders of ε . Equation (29) was also proposed and studied in [Vandekerckhove et al., 2011] (called INITMAN by Vandekerckhove et al. [2011]).

8 Discussion of the convergence statements

Adaptation of restriction R and lifting L Theorem 1 is a local statement with respect to x , claiming convergence only in a region $\text{dom } L$ in which the transversality conditions are uniformly satisfied, and restricting the times δ and t such that the slow flow $M_\varepsilon(\cdot; g_\varepsilon(x))$ cannot leave the slightly larger region $\text{dom } R$ for the times δ and $\delta + t$. This is appropriate because in many cases, during continuation or projective integration the maps R and L get adapted along curves of equilibria or along trajectories.

Testing the transversality conditions and choosing the healing time and coarse dimension The conditions S1, S2, M1 and M2 listed in contain terms that are unknown in practice. For example, the fiber projection g_0 and the tangent space $\mathcal{T}_0(u)$ to the slow manifold are both inaccessible because in many cases one can not vary the time scale separation parameter ε . However, observing the minimal singular value of the linearization $\partial/\partial x[RM_\varepsilon(\delta; Lx)]$ with respect to x (an n -dimensional matrix) serves as an indicator: in points where the transversality condition is violated, the linearization becomes singular.

Similarly, the condition of the linearization, $K_\delta = \text{cond } \partial/\partial x[RM_\varepsilon(\delta; Lx)]$, is a guide how to choose an optimal healing time δ . While the error due to finite time scale becomes smaller at a faster rate than K_δ grows, other errors may become dominant when they are amplified by K_δ . Especially, when the microscopic system is a Monte-Carlo simulation, a trajectory $M_\varepsilon(t; u)$ is determined via ensemble runs, and the accuracy of the evaluation of M_ε is only of the order of $1/\sqrt{S}$ where S is the ensemble size.

The linearization $\partial/\partial x[RM_\varepsilon(\delta; Lx)]$ also helps to discover if one has too many coarse variables, that is, if n is too large such that the flow M_ε restricted to the assumed slow manifold \mathcal{C}_ε is not sufficiently slow (still containing rapidly decaying components). Then $\partial/\partial x[RM_\varepsilon(\delta; Lx)]$ becomes close to singular, too. Note that any solution found, for example, by solving the fixed point equation (26) is still a correctly identified fixed point

with correctly identified stability. However, the linearization of (26) becomes close to singular.

Stochastic systems Barkley et al. [2006] analysed how the equation-free approach can be used to analyse moment maps of stochastic systems or high-dimensional chaotic systems that converge in a statistical mechanics sense to low-dimensional stochastic differential equations (SDEs). They observe that the healing time strongly influences the results. Even the inclusion of additional macroscopic variables (increasing n) drastically changed the results of the equation-free analysis. It is unclear, how the implicit scheme (23) behaves in the situations studied by [Barkley et al., 2006]. While Barkley et al. [2006] also invoke a separation-of-time-scales argument to study approximation quality, their setting does not fit into the assumptions underlying Fenichel’s theorem, but requires weaker notions of convergence (see [Givon et al., 2004] for a review).

9 Test examples

9.1 A prototype slow-fast system of ODEs

We demonstrate the convergence properties using a simple slow-fast system of two fast variables and two slow variables. We denote the components of the variable u by (x, y) , where $x = (x_1, x_2)$ and $y = (y_1, y_2)$.

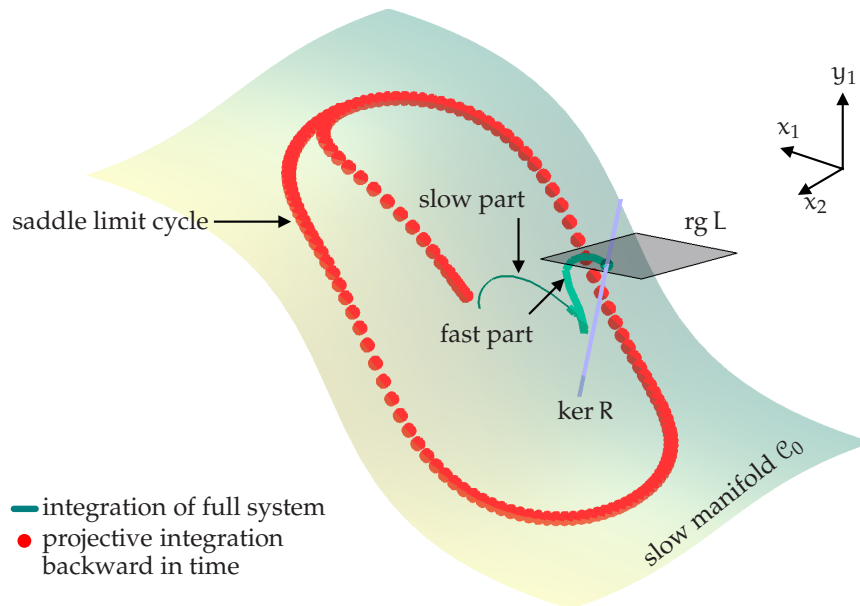


Figure 5: Phase portraits and slow manifold of the four-dimensional slow fastsystem (31)–(30). Parameters: $\mu = -4$, $\varepsilon = 10^{-2}$, $\delta = \sqrt{\varepsilon} = 10^{-1}$, $h = 10^{-2}$, $H = -0.05$, $\theta_R = 0.2$, $\theta_L = -0.2$.

The fast subsystem is linear in y , and the overall system has the form in the fast time scale

$$\dot{x}(t) = \varepsilon f(x, y) + h(y - g(x)), \quad (30)$$

$$\dot{y}(t) = -A_y (y - g(x)), \quad (31)$$

where A has a complex pair of eigenvalues with positive real part. For the illustration in Figure 5 we choose

$$A_y = \begin{bmatrix} 0 & -1 \\ 5 & 2 \end{bmatrix}, \quad \text{and} \quad g(x_1, x_2) = \begin{bmatrix} \operatorname{asinh} 2x_1 - \operatorname{asinh} x_2 \\ \operatorname{asinh} x_2. \end{bmatrix}$$

such that the eigenvalues of A_y are $1 \pm 2i$, and the slow manifold is the graph

$$\mathcal{C}_0 = \{(x, y) : y = g(x)\}.$$

For the slow dynamics, determined by f , we use the subcritical Hopf normal form but replace x in several places with $\tilde{x} = g^{-1}(y)$ (note that our g is invertible):

$$\begin{aligned} f_1(x, y) &= \mu \tilde{x}_1(y) - x_2 + \tilde{x}_1(y) [x_1^2 + x_2^2] \\ f_2(x, y) &= x_1 + \mu x_2 + x_2 [\tilde{x}_1(y)^2 + x_2^2], \end{aligned} \quad (32)$$

where $\tilde{x}_1(y_1, y_2) = \sinh(y_1 - y_2)/2$. The additional term $h(y - g(x))$ in (30) puts the slow-fast system into general position: the fast dynamics no longer changes only y but also x , mimicking the case where the decomposition into fast variables and slow variables is not known precisely. We choose

$$h(y) = \frac{(y_1^3, y_2^3)}{(1 + y_1^4 + y_2^4)^{3/4}}$$

such that the h -term in (30) does not alter the local stability of the slow manifold \mathcal{C}_0 , and the h -term stays globally bounded.

In the limit $\varepsilon \rightarrow 0$ the reduced system for (30)–(31) follows the subcritical Hopf normal form on the slow time scale (using prime to indicate slow time scale):

$$\begin{aligned} x_1' &= \mu x_1 - x_2 + x_1 [x_1^2 + x_2^2] \\ x_2' &= x_1 + \mu x_2 + x_2 [x_1^2 + x_2^2], \end{aligned}$$

which has a stable fixed point at the origin, $x = 0$, and an unstable periodic of radius 2 at our choice of μ , $\mu = 2$, $(x_1(t), x_2(t)) = (x_3(t), x_4(t)) = (2 \cos(t + \varphi), 2 \sin(t + \varphi))$, as its only recurrent sets. These sets persist in the coupled singularly perturbed system (30)–(31) for $\varepsilon > 0$ and live on the invariant manifold \mathcal{C}_ε . Figure 5 shows this unstable

periodic orbit as obtained using projected integration on the slow manifold *backward in time* with the trapezoidal rule:

$$\begin{aligned} \text{RM}_\varepsilon(\delta; \text{L}x_{j+1}) - \text{RM}_\varepsilon(\delta; \text{L}x_j) = \frac{H}{2h} \left[\text{RM}_\varepsilon(\delta + h; \text{L}x_{j+1}) - \text{RM}_\varepsilon(\delta; \text{L}(x_{j+1})) + \right. \\ \left. + \text{RM}_\varepsilon(\delta + h; \text{L}x_j) - \text{RM}_\varepsilon(\delta; \text{L}(x_j)) \right]. \end{aligned} \quad (33)$$

Note that the terms $M_\varepsilon(\delta; \text{L}x)$ can be computed as part of $M_\varepsilon(\delta + h; \text{L}x)$. We remark that integration backward in time is practically impossible for the full system (30)–(31) because the invariant manifold \mathcal{C}_ε is strongly unstable after reversal of time.

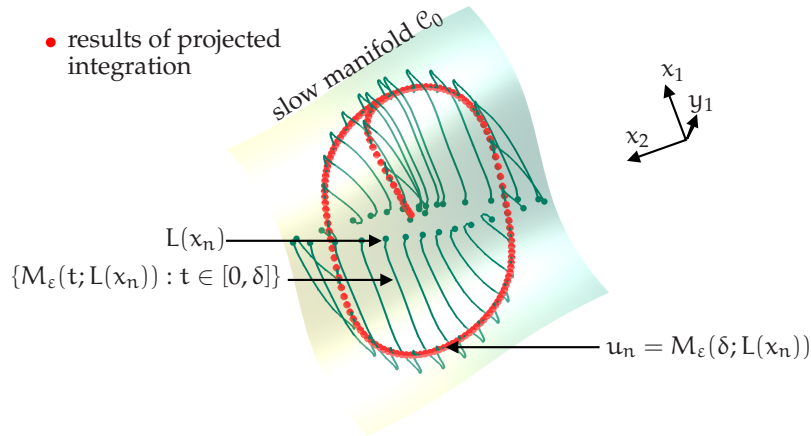


Figure 6: Zoom into phase portrait Figure 5 (look from above onto the slow manifold \mathcal{C}_0), illustrating the large healing correction to $L(x)$, obtained by applying $u \mapsto M_\varepsilon(\delta, u)$ (the illustration shows only every fifth computed point). Parameters: $\mu = -4$, $\varepsilon = 10^{-2}$, $\delta = \sqrt{\varepsilon} = 10^{-1}$, $h = 10^{-2}$, $H = -0.05$, $\theta_R = 0.2$, $\theta_L = -0.2$.

9.2 Investigation of dependence on L and R

For the projected integration scheme (33) we have to specify the lifting L and the restriction R:

$$\begin{aligned} \text{R}u = \text{R}(x, y) &= (1 - \theta_R)x + \theta_R y, \\ \text{L}x &= \begin{bmatrix} (1 - \theta_L)x + \theta_L x_{\text{ref}} \\ (1 - \theta_L)y_{\text{ref}} + \theta_L [x - x_{\text{ref}}] \end{bmatrix} \end{aligned} \quad (34)$$

Both definitions contain a parameter, θ_L and θ_R , which control the angle of both projections relative to the slow manifold. One natural choice for R and L for example (30)–(31) would be $\theta_R = \theta_L = 0$, effectively picking x as the slow variable and y as the fast variable. The lifting L also depends on a reference value $u_{\text{ref}} = (x_{\text{ref}}, y_{\text{ref}})$. This reference value permits to place the lifted value $\text{L}x$ close to the slow manifold, which may be

important if the slow manifold is not globally stable. A natural choice for projected integration is $u_{\text{ref}} = M_\varepsilon(\delta; Lx_{n-1})$, the image of the previous point along the projected trajectory under $M_\varepsilon(\delta; L(\cdot))$. In the example, we make the naive choice $u_{\text{ref}} = 0$ such that

$$Lx = \begin{bmatrix} (1 - \theta_L)x \\ \theta_L x \end{bmatrix}.$$

Figure 6 shows that this forces the operator $u \mapsto M_\varepsilon(\delta; u)$ to make large corrections to the lifted value Lx_n . We have an accurate approximation for the local error of the

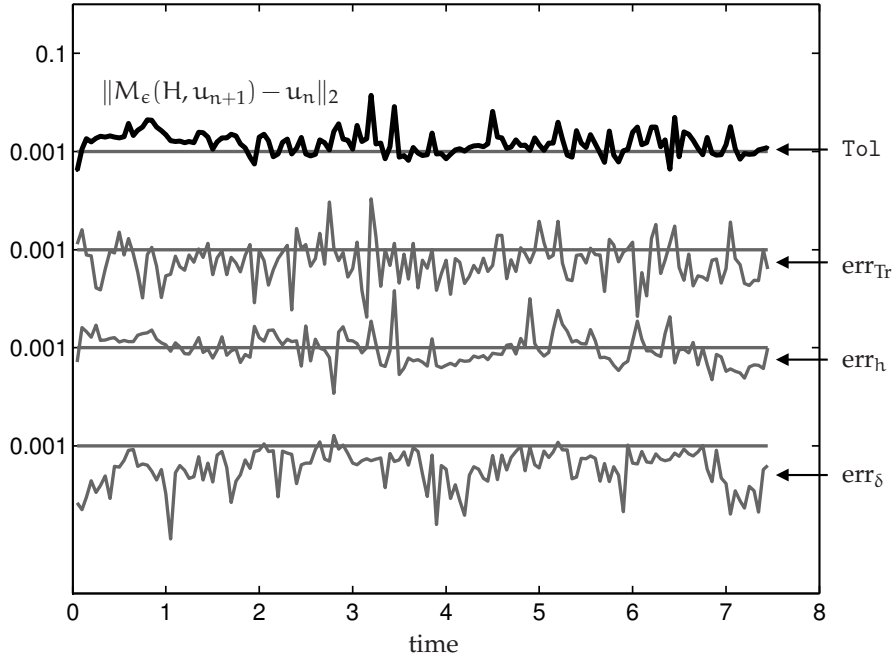


Figure 7: Local error $\tilde{u}_n - u_n$ of projected backward integration (curve at the top). Shown below are estimates for the various sources of error: the tolerance Tol of the time stepper (10^{-3}), the local error err_{Tr} of the trapezoidal rule, approximation error err_h for right-hand side, and the error err_δ due to incomplete healing. Parameters: $\mu = -2$, $\varepsilon = 10^{-2}$, $\delta = \sqrt{\varepsilon} = 10^{-1}$, $h = 10^{-2}$, $H = -0.05$, $\theta_R = 0.2$, $\theta_L = -0.2$.

projected backward integration (33): we can, after performing one projected integration step backward in time (with $H = -0.05 < 0$) from u_n to u_{n+1} , perform a forward integration step with the time stepper, $\tilde{u}_n = M(-H; u_{n+1})$ (recall that $H < 0$), and compare u_n and \tilde{u}_n for every n . Figure 7 shows the norm of the difference $\tilde{u}_n - u_n$ (black line at the top) along with estimates for the sources of error introduced at different stages of approximation. The four contributions to the overall error are:

- the accuracy of the time stepper. Figure 7 shows the chosen tolerance Tol (10^{-3}) set as an option to the used integrator `ode15s`.

- The local discretization error err_{Tr} when applying projected integration with a numerical method (in the example the trapezoidal rule), that is, the error occurring in each step when approximating (20) by the discrete iteration (33). The estimate shown in Figure 7 was obtained by checking the difference between u_{n+1} and \hat{u}_{n+1} , obtained by applying two steps of the trapezoidal rule with stepsize $H/2$, starting from u_n . Assuming that the local error of the trapezoidal rule is of order H^3 we estimate $\text{err}_{\text{Tr}} = (8/7)\|u_{n+1} - \hat{u}_{n+1}\|_2$.
- The error err_h incurred when approximating the right-hand side $[F_\varepsilon](u)$ by a discretization, $[M_\varepsilon(h; u) - u]/h$. We estimate this error by assuming that it has order 1 such that

$$\text{err}_h = 2 \left\| \frac{1}{h} [R(M_\varepsilon(h; u_n)) - R(u_n)] - \frac{2}{h} [R(M_\varepsilon(h/2; u_n)) - R(u_n)] \right\|$$

in Figure 7.

- The healing error err_δ incurred when approximating the dynamics on the slow invariant manifold \mathcal{C}_ε , that is, the error occurring when approximating Φ_* , defined by (21), with Φ , defined by (23). In general one does not have a direct estimate for this component. However, in the example, we can evaluate the distance from the second-order approximation of the slow manifold:

$$\text{err}_\delta = \|y_n - g(x_n) + \varepsilon A_y^{-1} g'(x_n) f(x_n, g(x_n))\|.$$

Note that this is not the true distance from the approximate manifold \mathcal{C}_ε , given by

$$\mathcal{C}_\varepsilon = \{(x, y) : y = g(x) - \varepsilon A_y^{-1} g'(x) f(x, g(x)) + O(\varepsilon^2)\},$$

but it is an upper bound.

Figure 7 shows that the local error at every step has the magnitude expected from the contributions of approximations performed during the projected integration. Figure 8 shows a measure for the global error and its dependence on the choice of lifting and restriction. The original system has a periodic orbit of saddle type which the projected integration converges to as the number of steps increases. This periodic orbit has a transverse intersection with the plane $\mathcal{P} = \{u = (x, y) : x_2 = u_2 = -1.5\}$ near $u_1 (= x_1) = 1.3$. Clearly, the sequence $u_n = M_\varepsilon(\delta; Lx_n)$, generated by the projected integration, depends strongly on L and R , which in our example have the parameter θ_L and θ_R :

$$\Delta u_n \sim (\Delta\theta_R, \Delta\theta_L).$$

However, the location of the intersection of the interpolated sequence u_n with \mathcal{P} should be independent of θ_R and θ_L . This intersection should approximate the intersection of the periodic orbit with \mathcal{P} because the orbit is attracting backward in time within the slow manifold \mathcal{C}_ε and attracting forward in time along the stable fibres of \mathcal{C}_ε . Figure 8

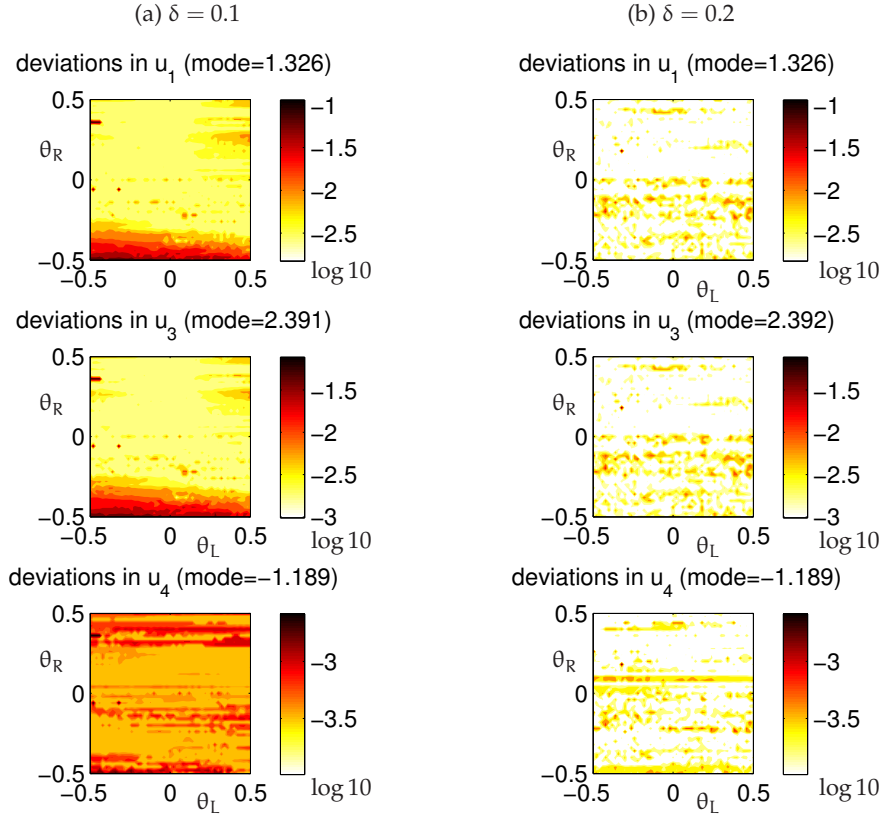


Figure 8: Dependence of results on tilt θ_L of lifting L and tilt θ_R of restriction R.

shows how the quality of the approximation depends on the choice of L and R (through varying the parameters θ_L and θ_R) for two different healing times δ . We note that the choice of healing time is limited in this example because trajectories blow up to infinity in finite time backward in time on the slow manifold \mathcal{C}_ε . A healing time of $\delta = 0.2$ was the maximal value that avoided blow-up along the entire projected orbit. We can see that the error is independent of the parameters over large ranges but that the error increases close to $\theta_R = -0.5$ (see, for example, the deviations in u_1 and u_3 in Figure 8(a) for $\delta = 0.1$). This is to be expected: the transversality conditions M1 on L and M2 on R can be violated along hypersurfaces in the phase and parameter space, which the orbit may intersect along the projected integration. Thus, in practical examples the transversality has to be monitored, and possibly, the restriction and lifting have to be adapted.

References

D. Barkley, I. G. Kevrikidis, and A. M. Stuart. The moment map: nonlinear dynamics of density evolution via a few moments. *SIAM Journal on Applied Dynamical Systems*, 5(3):

403–434, 2006.

N Fenichel. Geometric Singular Perturbation Theory for Ordinary Differential Equations. *Journal of Differential Equations*, 31:53–98, 1979.

C. W. Gear, T. J. Kaper, I. G. Kevrekidis, and A. Zagaris. Projecting to a slow manifold: Singularly perturbed systems and legacy codes. *SIAM Journal on Applied Dynamical Systems*, 4:711–732, 2005. doi: 10.1137/040608295. URL <http://link.aip.org/link/?SJA/4/711/1>.

Dror Givon, Raz Kupferman, and Andrew Stuart. Extracting macroscopic dynamics: model problems and algorithms. *Nonlinearity*, 17(6):55–127, 2004.

Thilo Gross and Ioannis G Kevrekidis. Robust oscillations in sis epidemics on adaptive networks: Coarse graining by automated moment closure. *EPL (Europhysics Letters)*, 82(3):38004, 2008.

Thilo Gross, Carlos J. Dommar D’Lima, and Bernd Blasius. Epidemic dynamics on an adaptive network. *Phys. Rev. Lett.*, 96:208701, 2006. doi: 10.1103/PhysRevLett.96.208701. URL <http://link.aps.org/doi/10.1103/PhysRevLett.96.208701>.

Y. Kevrekidis and G. Samaey. Equation-free modeling. *Scholarpedia*, 5(9):4847, 2010.

Yannis Kevrekidis and Giovanni Samaey. Equation-free multiscale computation: algorithms and applications. *Review of Physical Chemistry*, 60:321–344, 2009.

C. Marschler, J. Sieber, R. Berkemer, A. Kawamoto, and J. Starke. Implicit methods for equation-free analysis: convergence results and analysis of emergent waves in microscopic traffic models. *preprint*, 2013. URL <http://arxiv.org/abs/1301.6044>.

Christophe Vandekerckhove, Benjamin Sunday, Alexei Makeev, Dirk Roose, and Ioannis G. Kevrekidis. A common approach to the computation of coarse-scale steady states and to consistent initialization on a slow manifold. *Computers & Chemical Engineering*, 35(10):1949 – 1958, 2011. ISSN 0098-1354. doi: 10.1016/j.compchemeng.2010.12.002. URL <http://www.sciencedirect.com/science/article/pii/S0098135410003637>.

A. Zagaris, C. Vandekerckhove, C. W. Gear, T. J. Kaper, and I. G. Kevrekidis. Stability and stabilization of the constrained runs schemes for equation-free projection to a slow manifold. *Discrete and Continuous Dynamical Systems - Series A*, 32(8):2759 – 2803, 2012.

Antonios Zagaris, C. William Gear, Tasso J. Kaper, and Yannis G. Kevrekidis. Analysis of the accuracy and convergence of equation-free projection to a slow manifold. *ESAIM: Mathematical Modelling and Numerical Analysis*, 43(04):757–784, 2009. doi: 10.1051/m2an/2009026. URL <http://dx.doi.org/10.1051/m2an/2009026>.